Designing, characterization, and application of cross-linked chitosan possessing Schiff base and ion-imprinted network polymer for selective removal of Cu(II) from aqueous solution

Huda Y. Sharef*, Nabil A. Fakhre

*Department of Chemistry, College of Education, Salahaddin University-Erbil, Erbil, Iraq, Tel. +9647504994900;
emails: huda.sharef@su.edu.krd (H.Y. Sharef), nabil.fakhre@su.edu.krd (N.A. Fakhre)*

ABSTRACT

Shrimp shells are an abundant natural resource for chitosan generation as bio sorbent. In this work, imine was prepared through the modified free amino group $-NH_2$ of chitosan using 4-fluorobenzaldehyde. The ion-imprinted method was used to prepare a new bulk polymer as a selective, fast, high-performance approach to remove copper ions. Adsorbents were characterized using Fourier-transform infrared spectroscopy, scanning electron microscopy, energy-dispersive X-ray, X-ray powder diffraction, transmission electron microscopy, and nuclear magnetic resonance techniques. Operational parameters including pH, contact time, adsorbent quantity, metal concentration, and temperature were evaluated. Results illustrated Cu(II) adsorption by Cu(II) ion-imprinted polymers (Cu(II)-IIP) is independent pH. The kinetic and isotherms dada fitted well to second-order reaction and Langmuir model with the maximum adsorption capacities of 20.8 mg/g for imine and 22 mg/g for Cu(II)-IIP at pH 8.0. Thermodynamic parameters ($\Delta G° < 0$ and $\Delta H° > 0$) suggested a spontaneous and endothermic adsorption process. The recycling and reuse showed that imine retained its adsorption capacity for Cu(II) ions after four consecutive cycles, while Cu(II)-IIP showed high efficiency and no significant decrease for copper removal after ten cycles.

Keywords: Cross-linked chitosan; Schiff base; Cu(II); Ion-imprint; Sorption; Uptake kinetics

1. Introduction

Heavy metals have been classified as a hazardous contaminant for human and environment due to their adverse effects, including toxicity, non-biodegradation, bioaccumulation, bio-transportation, carcinogenesis and quick spread to large area [1]. Ni(II), Zn(II), Ag(II), Pb(II), Fe(II), Cr(III), Cu(II) and Cd(II) are the main heavy metals in industrial wastewater effluent. However, Cu(II) is present in high concentrations in wastewater due to its wide application in various industries such as metal finishing, electroplating, plastics, and etching [2]. Although Cu(II) is an essential trace element that is essential for body metabolism in low amounts, exposure to its high amount could lead to serious diseases, especially in children [1]. United State Environmental Protection Agency (USEPA) and World Health Organization (WHO) have recommended the Cu(II) content in drinking water less than 1.3 and 2 mg/L, respectively [2]. Therefore, the separation and removal of copper ions as an important contaminant from water sources using effective procedures are needed to provide safe water [3].

Different methods have been utilized for removal of heavy metals including chemical precipitation, membrane filtration, ion exchange, electrolysis and adsorption. The application of each method could be restricted by several drawbacks such as secondary contamination, limited processing capacity, high cost, poor selectivity, and high energy

* Corresponding author.

consumption. Affordability and selectivity problems are also present in a low-cost, pollution-free technology now under development [4]. Compared to other methods, adsorption is more cost-effective and environment-friendly [5]. Currently available adsorbents include bio sorbents generated from renewable natural sources as well as different modified forms are developed for removal of heavy metal ions [6]. Chitosan (CS) and its derivatives as bio sorbent have high potential applications in the areas of environmental biotechnology due to the existence of various functional groups such as amino-acetamido groups, and primary and secondary hydroxyl groups which enhance the adsorption ability [7]. Chemical modifications are the principle approach that could be used to enhance the CS inhibitory effectiveness. For this aim amino groups of CS are combined with aldehyde derivatives to produce imines [8]. In the reaction between chitosan and aromatic aldehydes in an acetic acid medium, the reaction leads to the preparation of Schiff bases, Schiff base molecules that include an imine group (–RC=N–) [9].

Ion printing has attracted the attention of researchers because of its ability to have greater adsorption capacity and selectivity for metal ions. Different metal ions including zinc, copper, nickel, lead, dysprosium, etc. have been investigated for the imprinting process [9]. In the ion-imprinted polymers (IIPs) process, ions are used as templates to provide the particular recognition between template ions and functional monomers via electrostatic or coordination interactions. After cross-linking polymerization, the imprinted ions are eluted from the polymer with keeping its structure. Therefore, three-dimensional cavities with fixed size and shape will be produced that provide the selectivity removal of ions by the adsorbent [10]. This work aims to modify chitosan extracted from shrimp shells through reaction with 4-florobenzaldehyde to form high active imine as a strong sorbent in order to quickly take Cu(II) ions from an aqueous solution using small quantities. This work also covers the state-of-the-art in ion-imprinted technology, which has been accomplished either via the usage of the cross-linked imine with Cu(II) imprinting done through bulk polymerization. The operational parameters including contact time, initial Cu(II) concentration, pH, adsorbent dosage, and temperature were evaluated. Besides, bio sorbents were characterized by Fourier-transform infrared spectroscopy (FTIR), scanning electron microscopy (SEM), energy-dispersive X-ray (EDX), X-ray powder diffraction (XRD), transmission electron microscopy (TEM), and nuclear magnetic resonance (NMR) techniques.

2. Material and methods

2.1. Reagents

Chitosan (CS) (with DDA 69% from IR chart, M.W.: 15 kDa), 4-fluorobenzaldehyde (4-(F)C_6H_4CHO, CAS-Nr.: 459-57-4, M.W.: 124.11 g/mol), epichlorohydrin (EPI) (C_3H_5ClO, CAS-Nr: 106-89-8, M.W.: 92.53 g/mol), methanol (CH_3OH, CAS-Nr: 67-56-1, M.W.: 32.04 g/mol), sodium tripolyphosphate (TPP) ($Na_5P_3O_{10}$, CAS-Nr: 7758-29-4, M.W.: 367.864 g/mol), sodium hydroxide 1 N (NaOH, CAS-Nr: 1310-73-2, M.W.: 39.9971 g/mol), hydrogen chloride 1 N (HCl, CAS-Nr: 7647-01-0, M.W.: 36.46 g/mol), acetic acid (CH_3COOH, CAS-Nr: 64-19-7, M.W.: 60.052 g/mol), copper(II) sulfate hexahydrate ($CuSO_4$·6H_2O, CAS-Nr: 7758-99-8, M.W.: 267.7 g/mol), ethylenediaminetetraacetic acid (EDTA) ($C_{10}H_{16}N_2O_8$, CAS-Nr: 6381-92-6, M.W.: 292.244 g/mol) were purchased from BDH Middle East LLC (BDH), Merck, Sigma-Aldrich, and Scharlau Companies.

2.2. Chitosan extracted from shrimp shell

The chitosan was extracted using demineralization, deproteination, and deacetylation techniques. For this purpose, the shrimp shells were cleaned, dried, and crushed. Subsequently, it dissolved in hot water containing 4% (w/v) sodium hydroxide to dissolve proteins and sugars. The shell demineralization was conducted using 1% HCl for 24 h.

Finally, NaOH (50%) was added to the prepared mixture, and heated at 100°C for 2 h to finish the reaction process. The as-prepared sample was rinsed with tap water and distilled water to neutralize it and was dried in a vacuum oven at 60°C for 4–6 h [1,2].

2.3. Chitosan-Schiff base synthesis (imine)

The chitosan-Schiff base was produce according to the Vadivel et al. [3]. Briefly, 1.0 g chitosan powder was dissolved in 25 mL ethanol with 3 drops of acetic acid and vigorously stirred (sample A). Additionally, 4-fluorobenzaldehyde (0.87 g) was dissolved in 25 mL ethanol (sample B). Then sample B was added to sample A, agitated for 30 min and heated for 12 h in a 60°C under water bath. Finally, the obtained yellow product was filtered and dried after being rinsed with ethanol (3-(4-fluorobenzylidene)amino)-6-(hydroxymethyl)-2-methoxy-5-methyltetrahydro-2H-pyran-4-ol).

2.4. Cu(II) ion imprint polymer synthesis

The bulk polymerization approach has been applied in to generation of the Cu(II)-IIP. The polymer was synthesized in three steps with some modifications [4,5]. (i) 0.5 g imine with 10 mL D.W. and a few drops of CH_3COOH were mixed, then 5 mL $CuSO_4$·5H_2O (5,000 mg/L) was added to the mixture and stirred for 1 h at 30°C. (ii) The pH of as-prepared sample was adjusted to 7.0. Then, 1.0 mL epichlorohydrin (cross-linking reagent), 2.0 g of yeast, 10 mL TPP (2.5%), and 20 mL D.W. were added to the as-prepared sample and refluxed at 170°C for 18 h to produce the cross-linking reagent. Finally, the obtained polymer was filtered and washed many times with D.W. (iii) The Cu(II) ions present in the polymer network were eluted by 60 mL EDTA (0.1 M) at room temperature. The adsorbent was immersed in NaOH (0.1 M) for 1 h and washed many times with D.W. and acetone to remove the remaining epichlorohydrin. Finally, the obtained adsorbent was filtered and dried using the oven at 60°C.

2.5. Characterization of imine and Cu(II)-ion-imprinted polymer

The XRD analysis was utilized to determine the crystal structure and purity of adsorbents using Cu Kα radiation

(λ = 1.54 Å) at 2θ angle configuration scanning from 20° to 80°, with an applied current of 40 mA and a voltage of 45 kV. FTIR spectroscopy (Shimadzu IRAffinity-I FTIR) was used to evaluate the surface adsorption of functional groups (biomolecules) in the wavelength range of 400–4,000 cm^{-1}. Surface shape, morphology, and elemental composition of materials were studied using SEM (SEM Compact 6073) and EDX (Merlin Compact 6073) (Carl Zeiss, Germany) analyses. The size and morphology of the synthesized adsorbents were observed using the TEM (FEI Tecnai G2 F20). Finally, ^{1}H NMR (Bruker, AVANCE NEO 400 MHz) spectrometer was applied to examine the structure of molecules.

2.6. Adsorption procedure

The batch experiment was conducted as follows: sorbent dosage (10, 15, 20, 25, and 30 mg), pH (3–11), initial ion concentration (5–50 mg/L), contact time (0–24 h), and temperature (10°C–45°C). The 0.02 g adsorbents were added to solution content 10 mL of Cu(II), then stirred at room temperature. The residual concentration of Cu ion was determined using flame atomic absorption spectroscopy at 324.8 nm with a spectral bandwidth of 0.5 nm. The adsorption capacity was calculated according to Eq. (1):

$$q_e = \frac{(C_i - C_e)V}{M} \tag{1}$$

where q_e (mg/g) ions is equilibrium capacity, C_i (mg/L) and C_e (mg/L) are the initial and equilibrium concentration of metal ions, respectively. V (L) is the volume of solution, and the M (g) is the mass of the adsorbent. The selectivity of the adsorbent was evaluated by distribution coefficient according to Eq. (2):

$$K_d = \frac{q_e}{C_e} \tag{2}$$

where K_d (mg/L) is the distribution coefficient. The selectivity coefficient for the binding of a Cu(II) ions in the presence of competing species may be calculated using equilibrium binding data [Eq. (3)] [4].

$$K = \frac{K_d \text{Cu}(\text{II})}{K_d(M)} \tag{3}$$

where K denotes the selectivity coefficient and the metal ion denotes competing metals. When there are additional metals in the solution, they compete with each other in the adsorption process. K indicates Cu(II) ion adsorption selectivity. The higher value of K indicates the better the Cu(II) ions adsorption. Different isotherms including Freundlich, Langmuir and Temkin were used to investigate the mechanism of the adsorption process [6].

The Langmuir formula can be written with a linear form Eq. (4):

$$\frac{C_e}{q_e} = \frac{1}{q_m K_1} + \frac{C_e}{q_m} \tag{4}$$

where q_m is maximum capacity (mg/g). K_L is the Langmuir adsorption equilibrium constant (L/mg), which may be related to changes in the reasonably normal and porosity of the adsorbent that would lead to a higher adsorption ability for a bigger surface area and porous volume. In describing the basic characteristics of the Langmuir isotherm, the separation factor R_L, a dimensionless constant as illustrate in Eq. (5):

$$R_L = \frac{1}{1 + K_L C_o} \tag{5}$$

where R_L is the separation factor. R_L reveals data about the nature of adsorption: unfavorable ($R_L > 1$), linear ($R_L = 1$), when, favorable ($0 < R_L > 1$), and irreversible ($R_L = 0$). The linear form of the Freundlich isotherm is as Eq. (6):

$$\log q_e = \log K_F + \frac{1}{n} \log C_e \tag{6}$$

where K_f denotes adsorption capacity (L/mg) and $1/n$ representative adsorption intensity; it also denotes the energy distribution and adsorbate site heterogeneity.

Linear forms of the Temkin isotherm may be expressed by the following Eq. (7):

$$q_e = a_t + 2.303 b_t \log C_e \tag{7}$$

The Temkin constant (b_t) is related to the heat of sorption (J/mol) and the Temkin isotherm constant (a_t) (L/g).

The adsorption behavior during biosorption was investigated using a quasi-first-order kinetic model and a quasi-second-order kinetic model in this research [4].

Eq. (8) is quasi-first-order model:

$$\log(q_e - q_t) = \log q_e - \frac{K_1 t}{2.303} \tag{8}$$

Quasi-second-order model as explain by linear form Eq. (9):

$$\frac{t}{q_t} = \frac{t}{q_e} + \frac{1}{K_2 q e^2} \tag{9}$$

where K_1 is the quasi-first-order kinetic adsorption rate constant (1/min) and K_2 is the quasi-second-order kinetic adsorption rate constant (g/mg·min).

2.7. Real sample preparation

The efficiency of the imine and Cu(II)-IIP were evaluated with the determination of Cu(II) ion in some supplements. For this purpose, two types of supplements used by bodybuilders were evaluated. Firstly, heavy metals were digested using 1:3 HClO$_3$ and HNO$_3$, diluted with 10 mL D.W. and transferred into a tube containing adsorbent (0.02 g). The mixture was stirred in the thermostat water bath under optimum conditions. The adsorption and

recovery experiments were conducted for supplements by imine and Cu(II)-IIP.

3. Results and discussion

3.1. Characterization

3.1.1. Fourier-transform infrared spectroscopy

Fig. 1 shows the FTIR spectra of chitosan, imine and Cu(II)-IIP; the stretch of the OH and NH_2 functional groups is attributed to the wide peak at 3,570–3,330 cm^{-1}, whereas the stretching vibration of the (CH) group of the CS backbone is assigned to the peak at 2,885 cm^{-1}. The peaks associated with the amide group was observed at 1,083; 1,150, and 1,028 cm^{-1} (stretching vibration C–N bond), 1,383 cm^{-1} (stretching vibration C–O bond), and the absorption peak at 1,659 cm^{-1} [7,8]. The high absorbance band at 1,649 cm^{-1} is caused by C=N vibration typical of imine produced among the amino group of CS and the carbonyl group of aldehyde. The free aldehyde group is condensed along with a primary amine in the basic of the chitosan monomer, which produces Schiff base, no peak was seen between 1,720 and 1,740 cm^{-1} [3,9]. The FTIR results confirm cross-linked of Cu(II)-IIP with epichlorohydrin which has appeared in the peak of 1,255 cm^{-1} (C–O–C stretching) [7].

3.1.2. Scanning electron microscopy

The surface morphology of the adsorbents before and after adsorption was analyzed using the SEM. Results indicated the imine surface is rough and the small interspace structure to the metal in the solution may be readily absorbed by adsorbents (Fig. 2a). Results showed adsorption of Cu(II) by imine induce the dramatically changes of the adsorbent surface (Fig. 2b). Fig. 2c–e illustrate the SEM images of Cu(II)-IIP, polymer with copper (CuP) and non-imprinted polymer (NIP) respectively. Fig. 2c shows the presence of lots of porous with interconnecting pores in their network because of leached of Cu(II) ion as the templates in the synthesis process [8]. Fig. 2d indicates the cross-section
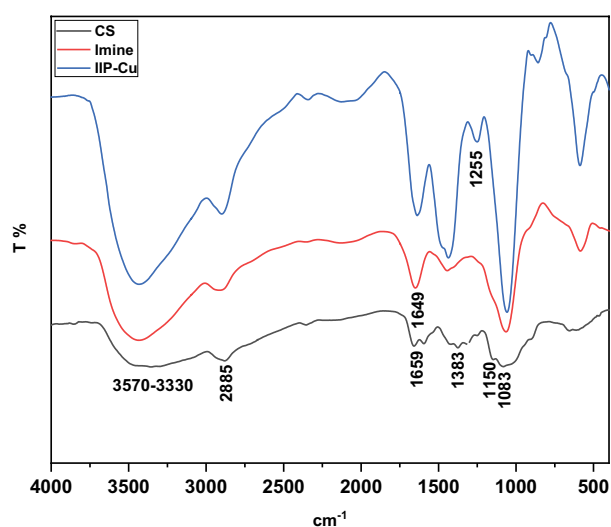
Fig. 1. FTIR for chitosan, imine and Cu-IIP.

and porous structures of CuP surface, while Fig. 2e shows smooth and non-cavity surface of NIP network polymer.

3.1.3. Transmission electron microscopy

Fig. 2. SEM pictures of imine (a) Cu adsorbed imine (b), Cu(II)-IIP (c), CuP (d) and NIP (e).

Fig. 3 shows the morphology and microstructure of imine (Schiff base), eluted IIP-Cu, and CuP after adsorption process respectively. Result indicated modified chitosan with 4-fluorobenzaldehyde is rough, bulk, and interspace molecules structure (Fig. 3a). Fig. 3b indicates the cavities (150 and 200 nm) that form during fabricated modified natural polymer (CS) with a highly cross-linked structure. these cavities can chelate with Cu ion to form imprinted excellent selectivity of Cu. Fig. 3c shows Cu(II)-IIP after adsorption (150 and 350 nm) with small dark areas indicating the presence of Cu ions in the cavities [8,10].

3.1.4. Energy-dispersive X-ray

The element composition of imine (a), imine-Cu ion (b), Cu(II)-IIP (c), CuP (d), and NIP (e) was analyzed by EDX analysis (Fig. 4). Fig. 4a indicates EDX analysis of imine. Fig. 4b illustrates the imine-Cu ion which confirms Cu(II) is successfully put on the imine surface. Fig. 4c shows the non-attendance of the Cu(II) in EDX-spectra which confirms Cu is leached completely from the polymer network by EDTA. This phenomenon provides the proper cavities for the adsorption of Cu(II) in the Cu(II)-IIP adsorbent. Moreover, Fig. 4e illustrates the lack of metal in non-ionic imprinted matrix.

3.1.5. X-ray powder diffraction

Fig. 5 indicates the imine, imine-Cu, Cu(II)-IIP and IIP. Results showed that compared to the imine, the crystalline structure of imine-Cu significantly changed indicating the adsorption behavior of the adsorbent caused by interaction between Cu(II) ion and $–CH_2OH$ binding site of chitosan [1,11,12]. While XRD analysis shows that there were no significant changes in peak locations, only an increase in intensity due to metal ion adsorption of ion imprinted net polymer, this indicates that the crystal structure of the net polymer was not destroyed after metal-ion adsorption (Fig. 5) [13].

3.1.6. Nuclear magnetic resonance

Fig. 6 shows the H NMR signal chemical shifts of the Schiff base – imine(3-((4-fluorobenzylidene)amino)-6-(hydroxymethyl)-2-methoxy-5-methyltetrahydro-2H-pyran-4-ol) recorded in DMSO. The spectrum provides the following signals: phenyl as a multiplex at 6.8–8 δ, $–N–CH_2$ at (4.5 δ), and C–CH=N– proton at 9.8 mg/L. This shifted occurrence in the spectrum on account of the high electronegativity of fluoride in the aromatic ring [12,14].

3.2. Adsorption time – kinetic study

Fig. 7a shows that the Cu(II) ion adsorption on imine and Cu(II)-IIP sharply increased up to 50 min and then
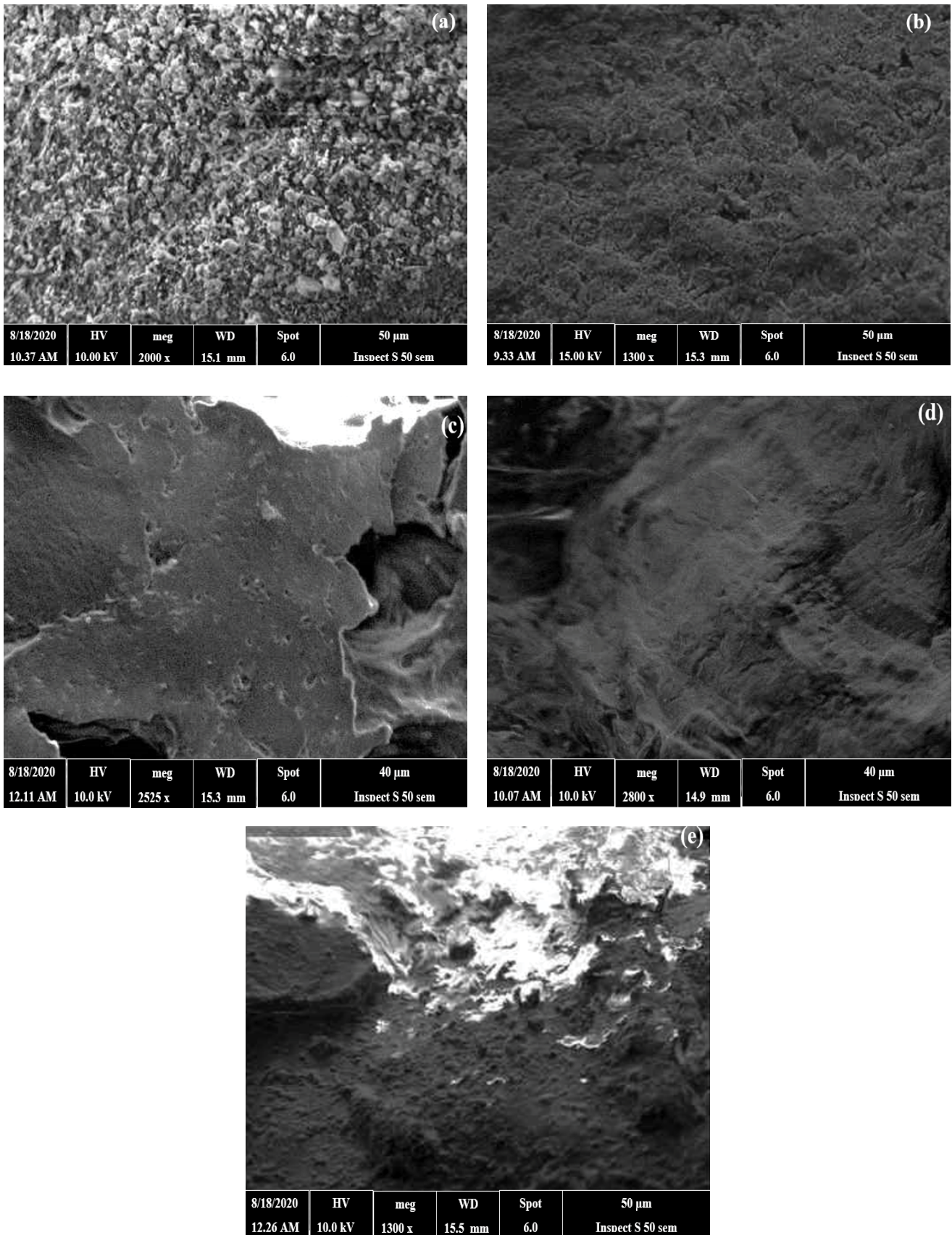
Fig. 2. SEM images of imine (a), imine-Cu(II) ion (b), Cu(II)-IIP (c), CuP (d) and NIP (e).
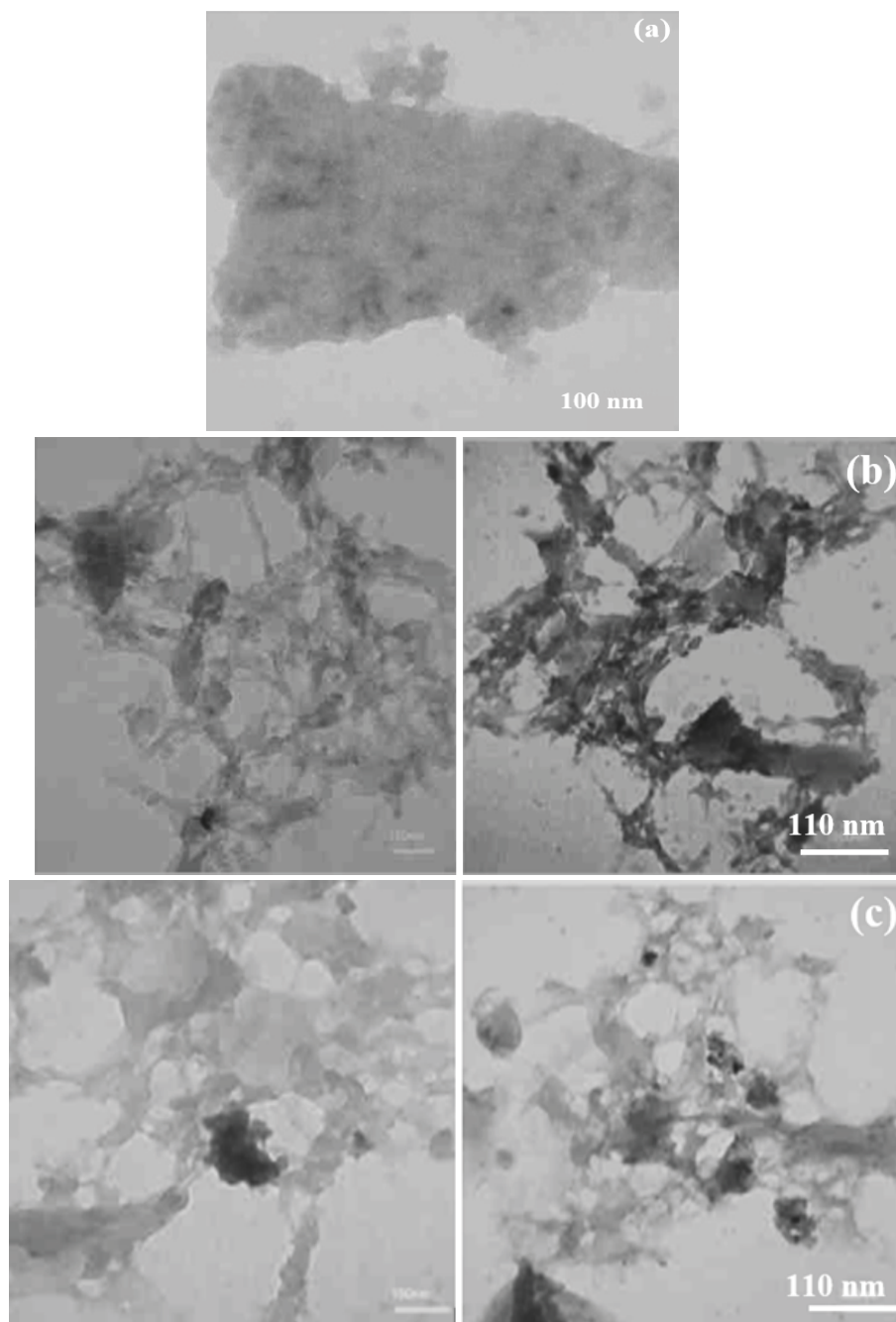
Fig. 3. TEM pictures of imine (a), Cu(II)-IIP (b) and CuP (c).

constant after 90 min (99%). This is due to an enormous number of specific active sites on the sorbent surface. Results also showed that the Cu(II) adsorption for Cu(II)-IIP (98.3%) is higher than imine (90) in 50 min. This is because of strong chelation and excellent affinity of Cu(II)-IIP sorbent were complementary in size and form toward a template ion. Two main kinetic models of quasi-first-order and quasi-second-order were used to investigate the mechanism of the processes; the details of the calculation rate constant (k), adsorption capacity, and correlation coefficient (R^2) are shown in the Table 1. Results indicated data are more fitted for quasi-second-order model compared to the quasi-first-

order model. Obeyed the experimental data of the quasi-second-order represents the chemisorption phenomenon, this includes valence forces created by electron sharing or exchange between the sorbent and the sorbate (Fig. 7c and e).

3.3. Effect of adsorption conditions

3.3.1. Effect of pH

pH is the main parameter in the adsorption process. Fig. 8 shows the effect of pH on Cu(II) adsorption by imine and Cu(II)-IIP. Results indicated the highest adsorption for
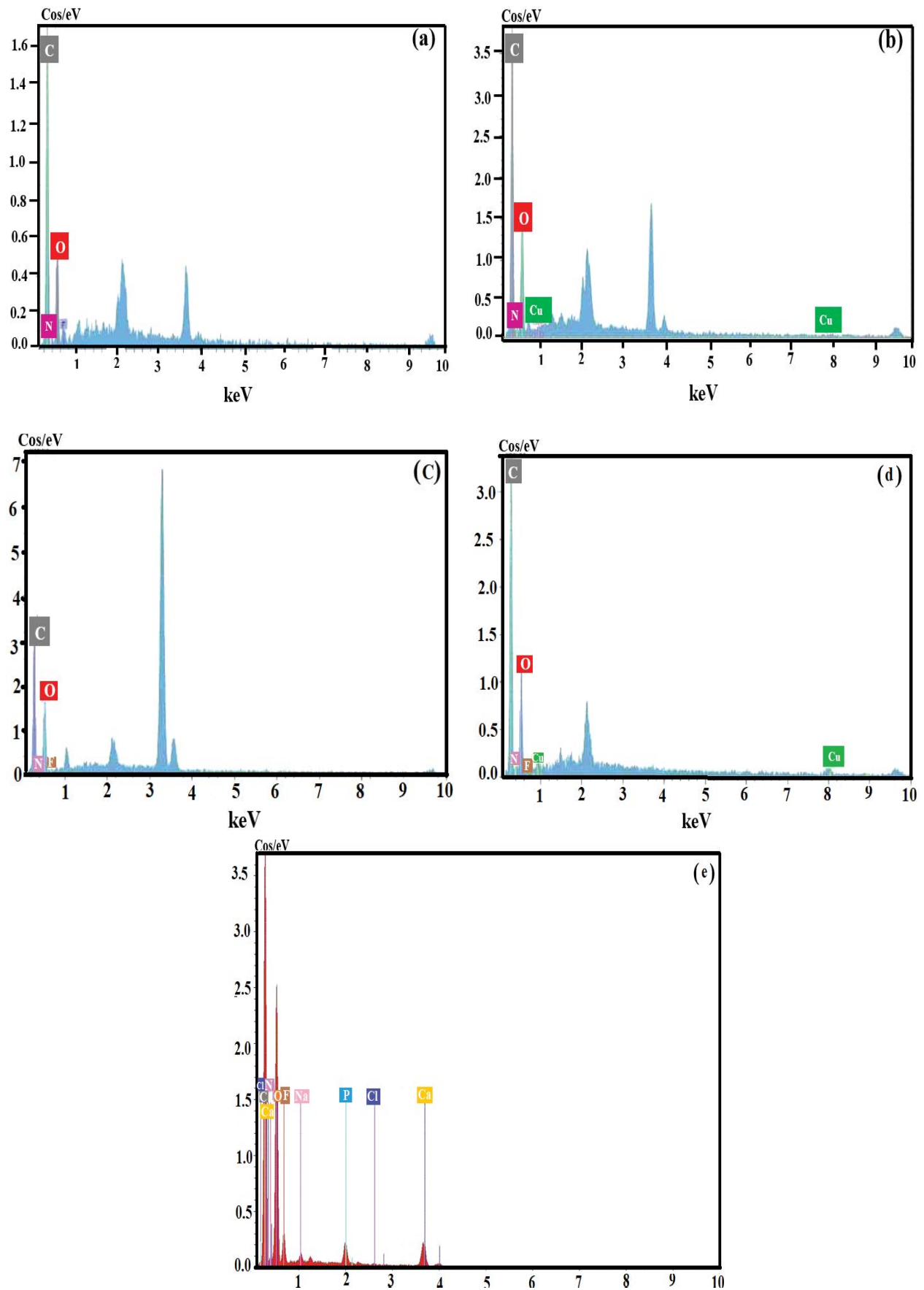
Fig. 4. EDX of imine (a), imine-Cu(II) ion (b), Cu(II)-IIP (c), CuP (d), and NIP (e).
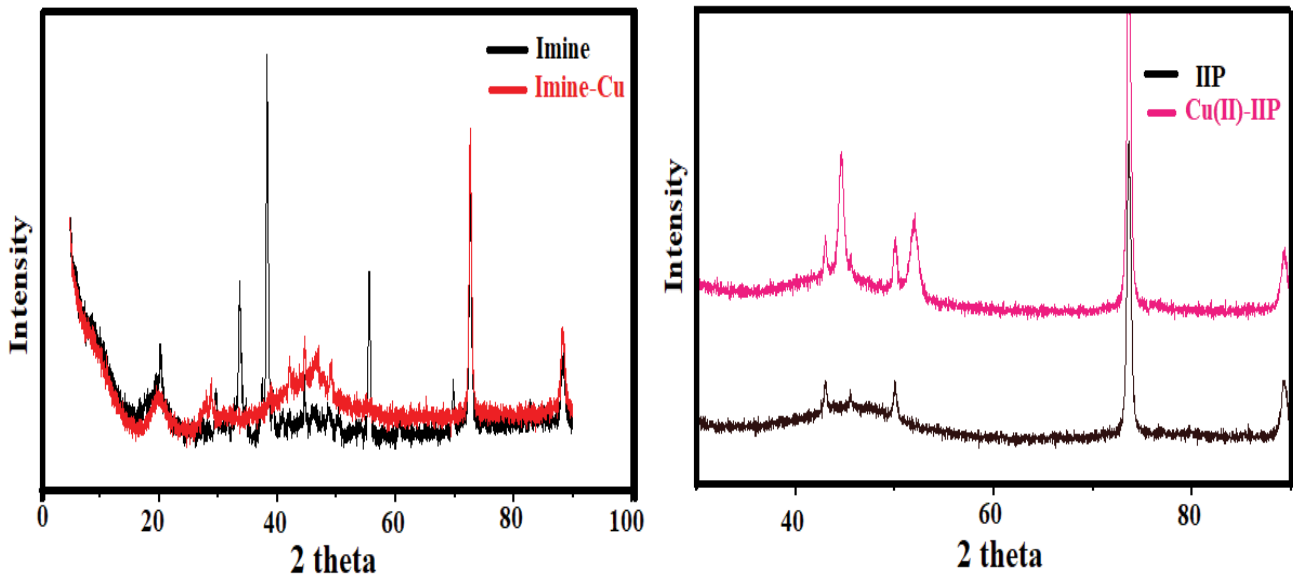
Fig. 5. XRD pattern of imine and Cu(II)-IIP biopolymer before and after Cu(II) adsorption.
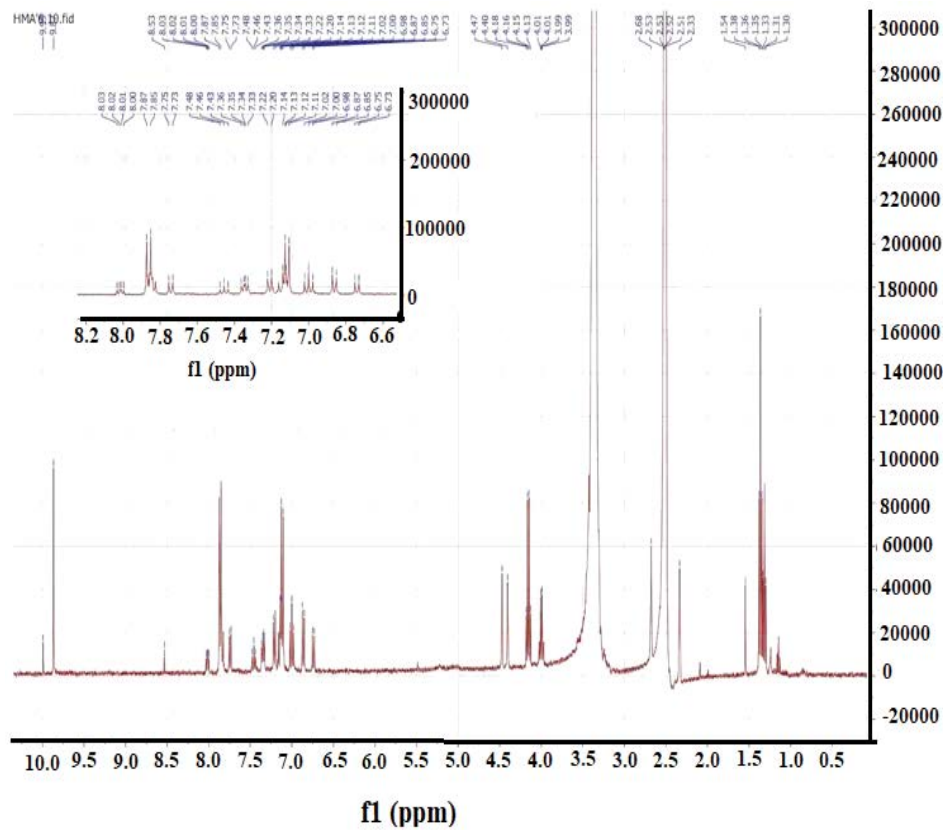
Fig. 6. H NMR for imine (3-((4-fluorobenzylidene)amino)-6-(hydroxymethyl)-2-methoxy 5-methyltetrahydro-2H-pyran-4-ol).

imine occur between pH 8 and 9. This is an expected effect because hydrogen ions compete with metallic ions for active sites on the natural sorbent surface. Moreover, protonation of the amino groups could occur at acidic pH and generate positively charged sites of the amino group which causes a repulsive force between the copper and the adsorbent. In contrast, increasing the pH leads to the increment of negatively charged active sites of adsorbent, this process enhanced the electrostatic attraction and improving the Cu(II) removal [15,16]. On the other hand, the removal
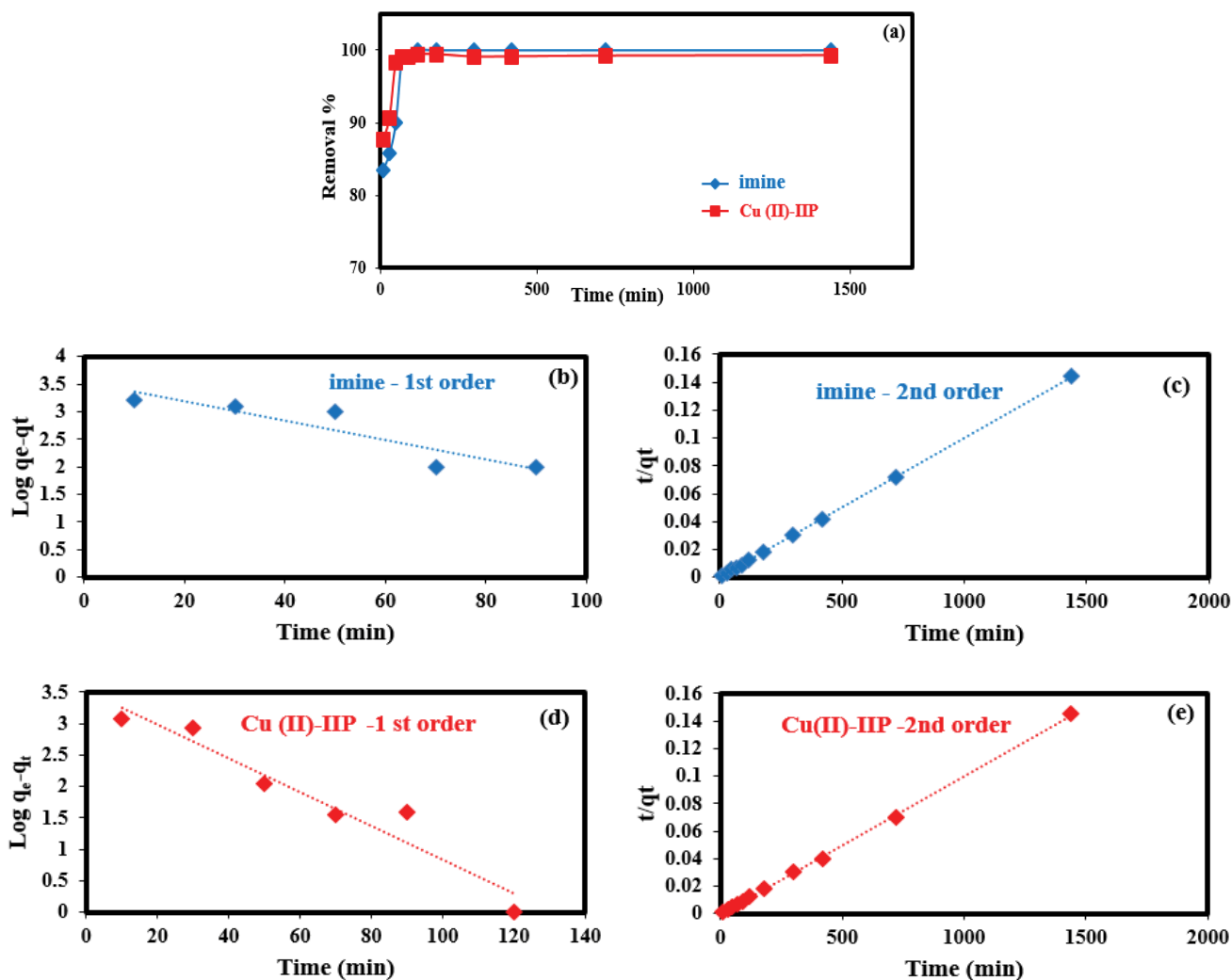
Fig. 7. Contact time (a), first-order imine-Cu(II) ion (b), second-order imine-Cu(II) ion (c) first-order Cu-IIP (d) and second-order Cu-IIP (e) models.

Table 1
Kinetic study parameters of imine-Cu(II) ions and Cu(II)-IIP first-order and second-order

Adsorbents	q_e (mg/g)	Quasi-first-order kinetic			Quasi-second-order kinetic		
		q_{cal} (mg/g)	$K \times 10^{-2}$ (min^{-1})	R^2	q_{cal} (mg/g)	$K \times 10^{-5}$ (g/mg·min)	R^2
Imine	10	3.4	4.0	0.832	10	5.0	1
Cu(II)-IIP	9.9	3.33	6.19	0.928	10	5.0	0.999

efficiency was decreased at pH > 9 because metal cations will deposit in hydroxides form at pH > 9. Therefore, pH 8 was chosen as the optimal [16]. Results showed the Cu(II) adsorption by Cu(II)-IIP is independent of pH and removal efficiency reached >97% in acidic, neutral, and basic conditions [17].

3.3.2. Effect of metal concentration

Fig. 9 shows the effect of the initial concentration of copper(II) (5–50 mg/L) on removal efficiency. Results showed

that the removal efficiency slightly increased by raising the initial concentration of copper(II) up to 30 mg/L (97%) and then drops slightly and remains almost constant. This is because of an adequate amount of active sites to occupy Cu(II) ions which leads to high removal efficiency for at low Cu(II) concentrations (<30 mg/L). Moreover, the driving force at a high concentration of pollutants can play a significant role in more diffusion of Cu(II) in adsorbent structure through overcoming mass transfer resistances between the liquid and solid-phase [18]. Contrary at higher initial Cu(II) concentrations and the same adsorbent mass, a scarcity
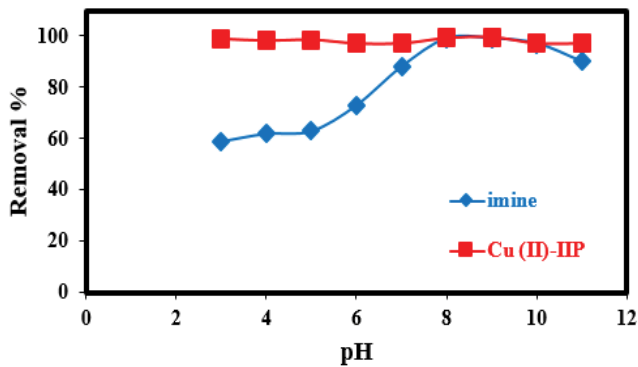
Fig. 8. pH effect Cu(II) ion on imine and Cu(II)-IIP.
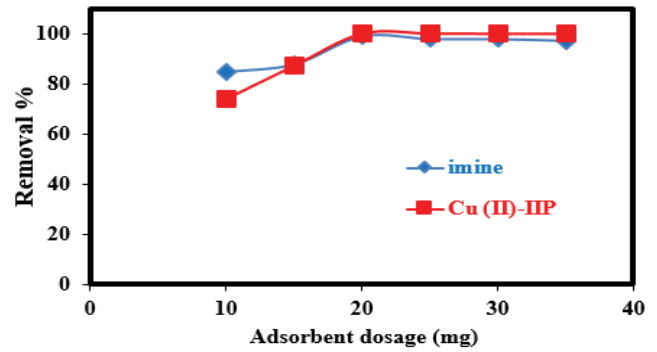
Fig. 10. Effect of dosage of imine and Cu(II)-IIP on Cu(II) adsorption.
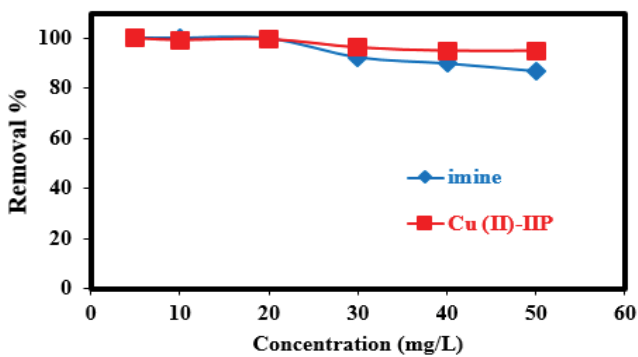
Fig. 9. Effect of initial concentration of Cu(II) ion on imine and Cu(II)-IIP.
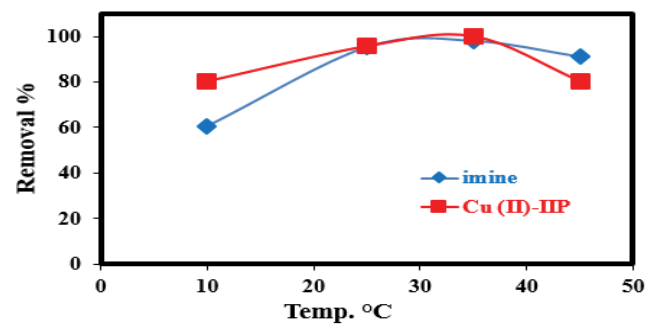
Fig. 11. Effect of temperature on Cu(II) ion adsorption by imine and Cu(II)-IIP.

of adsorption sites may develop, resulting in a decrease in removal effectiveness [8]. In addition, Cu(II) precipitation can occur at high concentrations under alkaline conditions, leading to a decrease in removal efficiency. However, as results indicated the removal efficiency for Cu(II)-IIP and even imine were slightly decreased. This phenomenon can be due to high capacity and sufficient active sites of adsorbent for removal of Cu(II) in 30 mg/L [18].

3.3.3. Effects of sorbent dose

Fig. 10 shows the effect of the sorbent dosage on Cu(II) using Schiff base and Cu(II)-IIP. Results indicated that the optimal sorbent dosage is 20 mg for both adsorbents and Cu(II) removal is 100% in the optimum condition. As Fig. 8 shows, the Cu(II) adsorption increases quickly with increases in the adsorbent dosage up to optimal dosage, and then removal efficiency is constant. This is due to an increase in the number of available active sites, which results in improved removal efficiency. The constant removal efficiency for high adsorbent dosage is due to adsorption site overlaps caused by adsorbent particle overpopulation [8,19].

3.3.4. Temperature effects

Temperature is the principal parameter in the adsorption process that affects the mobility of molecules and ions in a solution. Because ion adsorption must be mobile in

order to 'collide/interact' with the adsorbent and enhance adsorption process [20]. Fig. 11 shows the effect of temperature (10°C–50°C) on Cu(II) adsorption by imine and IIP-Cu. Results indicated the maximum removal efficiency (99%) of Cu(II) was obtained at 35°C. It could be concluded that the process is endothermic and rising temperatures enhance the adsorption of copper ions by adsorbent [21]. Therefore, with further increase in temperature (>45°C), the Cu(II) adsorption decreases due to Thinning of the upper layer which leads to metal ion egress from the adsorbent surface to the solution, this is why the adsorption decreases as temperature increases [22].

Enthalpy change ($\Delta H°$), Gibbs free energy change ($\Delta G°$), and entropy change ($\Delta S°$) are the thermodynamic parameters which employed to evaluate the spontaneity of the adsorption process. The following equations are used for calculating the thermodynamic parameters including thermodynamic equilibrium constant [Eq. (10)], standard Gibbs free energy $\Delta G°$ (kJ/mol), standard enthalpy change $\Delta H°$ (kJ/mol), and standard entropy change $\Delta S°$ [Eqs. (11) and (12)] [23,24].

$$K_d = \frac{q_e}{C_e} \tag{10}$$

$$\ln K_d = \frac{\Delta S}{R} + \frac{\Delta H}{RT} \tag{11}$$

$$\Delta G = -RT \ln K_d \qquad (12)$$

where K_d the adsorption distribution constant, R, ideal gas constant (8.314 J/mol·K); T, absolute temperature (K). The slope and intercept of the linear plot of $\ln K_d$ vs. $1/T$ were used to compute the ΔH and ΔS values, whereas the values of ΔG were determined using Eq. (12) [25]. Results indicated the adsorption of Cu(II) by imine and Cu(II)-IIP was more favorable at higher temperatures, implying that the adsorption process is endothermic, as shown by the positive values of ΔH (Table 2). The results suggest that chemisorption might be dominant. Moreover, a positive value of ΔS implies a high degree of randomness at the interface between the solid and the solution. The negative values of ΔG indicate that the adsorption of Cu(II) onto both biosorbents is spontaneous adsorption [24].

3.4. Isotherm models study

The equilibrium features for Cu(II) ions adsorption on imine and Cu(II)-IIP were calculated using Langmuir, Freundlich, and Temkin isotherms. Fig. 12 shows the linear regression of the Cu(II) adsorption isotherm models onto Schiff base and Cu(II)-IIP and Table 3 shows the factors and coefficients of correlation for Langmuir, Freundlich, and Temkin. Results indicated the Cu(II) adsorption by imine and Cu(II)-IIP correlated well ($R^2 > 0.99$) with Langmuir isotherm suggesting the adsorption mechanism is monolayer. High adsorption ability can be illustrated by higher values of K_L and R^2 for Cu(II)-imine (0.9987 and 12.327 L/mg) and Cu(II)-IIP polymer (0.9993 and 7.19 L/mg) indicating higher affinity between solute and adsorbent. Results also showed active sites are dealt with in a reasonably equal distribution on the surface and inside the adsorbent [4,25,26]. R_L, separation factor is favorable for imine and

Cu(II)-IIP toward Cu ion with range (0.0016–0.0159) and (0.0027–0.027) respectively.

3.5. Selectivity adsorption of Cu(II) ion

The selectivity adsorption of Cu(II) ion in the presence of different metals including Cu(II)/Fe(III), Cu(II)/Zn(II), Cu(II)/Co(II), Cu(II)/Cd(II), Cu(II)/Pb(II), Cu(II)/Ni(II) and Cu(II)/Cr(III) was investigated to assess the sensing of organic, imprinted metal frames. Both metal ions had the same concentration of 50 mg/L in their binary combination and 50 mg was utilized for sorbents. Selectivity factors include a coefficient of distribution (K_d) Eq. (2) and coefficient of selectivity (K) Eq. (3) [5]. Fig. 13 shows the removal percentage of Cu(II) with imine and Cu(II)-IIP in the presence of other ions. Table 4 indicates the selectivity coefficient (K) of Cu(II)/Fe(III), Cu(II)/Zn(II), Cu(II)/Co(II), Cu(II)/Cd(II), Cu(II)/Pb(II), Cu(II)/Ni(II) and Cu(II)/Cr(III) with imine and Cu(II)-IIP were significantly greater than one [27] It

Table 2
Thermodynamic parameters (ΔG, ΔH, ΔS) studies for the adsorption of Cu(II) ions onto imine and Cu(II)-IIP polymer

Adsorbents	T (K)	ΔG (kJ/mol)	ΔH (kJ/mol)	ΔS (J/mol·K)
Imine	283	0.616	+117.04	+408.55
	298	−5.74		
	308	−8.16		
	318	−4.28		
IIP-Cu	283	−1.68	+175.93	+618.05
	298	−5.89		
	308	−15.9		
	318	−1.86		
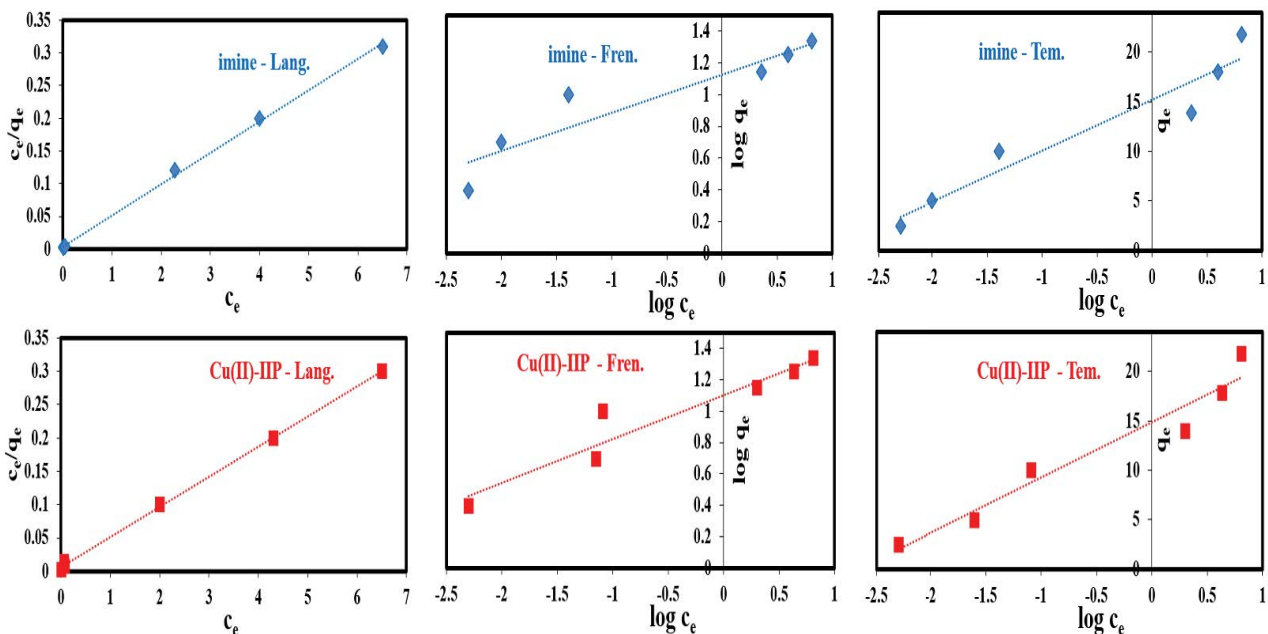
Fig. 12. Adsorption Cu(II) on imine and Cu(II)-IIP, Langmuir, Freundlich and Temkin isotherm model.

Table 3
Study of isotherm models correlation coefficients and constant for adsorption of Cu(II) on imine and Cu(II)-IIP

Adsorbent	Langmuir		Freundlich		Temkin	
	Parameter	Value	Parameter	Value	Parameter	Value
Imine (Schiff base)	q_m	20.8 mg/g	$1/n$	0.2397	a_t	15.196
	K_L	12.327	K_f	13.38	b_t	2.22
	R^2	0.9987	R^2	0.8718	R^2	0.927
	R_L	(0.0016–0.0159)				
Cu(II)-IIP	q_m	22 mg/g	$1/n$	0.2791	a_t	14.400
	K_L	7.19	K_f	12.6	b_t	2.832
	R^2	0.9993	R^2	0.917	R^2	0.8778
	R_L	(0.0027–0.027)				
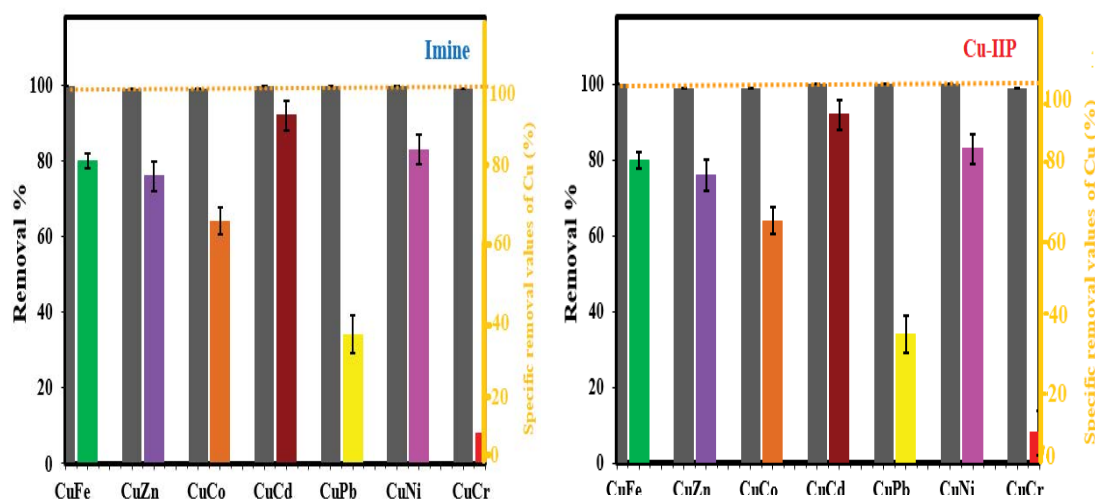
Fig. 13. Removal efficiency of Cu(II) in presence of other metals on imine and Cu(II)-IIP.

Table 4
Removal percent and selectivity factors of Cu(II) ion on imine-Schiff base and Cu(II)-IIP

Ions	Imine		Cu(II)-IIP	
	%	K	%	K
Cu	100	12.1	94	18.03
Fe	80		66	
Cu	99.7	97	97.8	12.97
Zn	77.2		77.3	
Cu	100	27	96.7	17.7
Co	64		62.6	
Cu	99.6	64	96.1	23.2
Cd	91.7		61.5	
Cu	99.2	267	95.8	33.9
Pb	33.3		40	
Cu	100	11.1	95.6	3.846
Ni	82.8		85	
Cu	99.5	612	98.7	159.8
Cr	2.26		4.5	

suggested that both organic–organic hybrid materials had higher sensing for Cu(II); this means that copper ions can be detected even in presence of other ions.

3.6. Desorption and reuse

Desorption and reused process are the main factors to evaluate the adsorbent's ability and stability. Desorption and reused processes for imine and Cu(II)-IIP were conducted with treating and dehydration of adsorbents using 0.1 M EDTA. The adsorption/desorption tests were carried out four times for imine and ten times for Cu(II)-IIP (Fig. 14). The findings revealed that the Cu(II)-IIP sorbent exhibited outstanding regeneration ability for Cu(II) without substantially decreasing activity, with a recovery rate of more >90%. While, the efficiency of imine was significantly reduced for cycle 3 and cycle 4 to 66% and 33%, respectively. The results suggested that Cu(II)-IIP has a better ability to reuse than the imine [4,9,28].

3.7. Comparison with another study

The adsorption capacity of imine used for removal of the ion Cu(II) was compared with the other adsorbents cited

in the literature. Table 5 shows the data compiled in the adsorption capacities obtained from the Langmuir model.

3.8. Application of real sample

A real sample was selected to evaluate the adsorbent ability in real conditions. Table 6 represents the two

Fig. 14. Adsorption–desorption of Cu(II) by imine I and IIP-Cu.

samples that were spiked with Cu(II) ions to supplement tablets. After the batch experiment the recovery of Cu(II) ion in real and spiked samples varied in the range 97.82%–99.80% ± 1.32 and 99.9%–100% ± 0.76 for III-Cu.

The results support the sensitivity and reliability of both adsorbents toward spike and non-spike for pre-concentration and determination of Cu(II) ion in trace values.

4. Conclusions

As a result, a new imine-Schiff base and a Cu(II)-IIP specific to one element has been generated and characterized using a variety of techniques (FTIR, EDX, XRD, SEM, TEM, H NMR) for surface morphology and chemical property. The research included investigating a variety of variables that influence adsorption rate to determine the optimal situation. The removal percent of Cu ion toward imine and Cu(II)-IIP were obtained 90% and 98%, respectively. Results illustrated Cu(II) adsorption by Cu(II)-IIP is independent pH. The kinetic and isotherms dada fitted well to second-order reaction and Langmuir model with the maximum adsorption capacities of 20.8 mg/g for imine and 22 mg/g for Cu(II)-IIP at pH 8.0. Thermodynamic parameters ($\Delta G° < 0$ and $\Delta H° > 0$) suggested a spontaneous and endothermic adsorption process. As a result, the selectivity coefficients

Table 5
Adsorption capacity of various adsorbents for Cu(II) removal

Adsorbents	Adsorption capacity (mg/g)	References
Itaconic acid, ethylene glycol dimethacrylate, and 2,20-azobisisobutyronitrile	16.12	[29]
Methacrylic acid (MAA) and vinylpyridine (4-VP)	22.2	[30]
4-vinylpyridine and methacrylic acid	0.99	
Dithizone, 3-aminopropyltriethoxysilane	1.058	[31]
	16.55	[32]
Chitosan cross-linked with Bisphenol A diglycidyl ether	17.539	[33]
Schiff base, 4-[(2-methoxybenzylidene)amino-2-phenyl]	5.64	[34]
Cryogels containing imidazole group	2.558	[35]
Imine-Schiff base	20.8	This work
Cu(II)-IIP	22.0	This work

Table 6
Determination of Cu(II) ion in some supplements and serums

Adsorbent	Samples	Amount added, µg/mL	Amount found, µg/mL	RSD	Recovery, %
Imine	Beta-hydroxy beta-methylbutyrate (HMB) supplement	0	15	±1.2	–
		30	44.8	±0.4	99.55
		50	64.3	±0.8	98.9
	Mv glutamine supplement	0	1	0	–
		30	30.94	±0.92	99.80
		50	49.89	±1.32	97.82
IIP-Cu	Beta-hydroxy beta-methylbutyrate (HMB) supplement	0	15	0	–
		30	44.99	±0.76	99.9
		50	64.97	0.54	99.95
	Mv glutamine supplement	30	131	0 ± 0.001	–100
		50	50.99	±0.1	99.98

of all copper(II)/interfering ions are more than one, showing that particular recognition sites for Cu(II) ions were created during the imprinting process. The results showed that Cu(II)-IIP has a high ability for reuse after 10 consecutive runs indicating that this new polymer has good stability and regeneration property.

References

[1] D.G. Trikkaliotis, A.K. Christoforidis, A.C. Mitropoulos, G.Z. Kyzas, Adsorption of copper ions onto chitosan/poly(vinyl alcohol) beads functionalized with poly(ethylene glycol), Carbohydr. Polym., 234 (2020) 115890, doi: 10.1016/j.carbpol.2020.115890.

[2] S.A. Al-Saydeh, M.H. El-Naas, S.J. Zaidi, Copper removal from industrial wastewater: a comprehensive review, J. Ind. Eng. Chem., 56 (2017) 35–44.

[3] T. Vadivel, M. Dhamodaran, S. Kulathooran, S. Kavitha, K. Amirthaganesan, S. Chandrasekaran, S. Ilayaraja, S. Senguttuvan, Rhodium(III) complexes derived from complexation of metal with azomethine linkage of chitosan biopolymer Schiff base ligand: spectral, thermal, morphological and electrochemical studies, Carbohydr. Res., 487 (2020) 107878, doi: 10.1016/j.carres.2019.107878.

[4] Y. Ren, M. Zhang, D. Zhao, Synthesis and properties of magnetic Cu(II) ion imprinted composite adsorbent for selective removal of copper, Desalination, 228 (2008) 135–149.

[5] J. Gatabi, Y. Sarrafi, M.M. Lakouraj, M. Taghavi, Facile and efficient removal of Pb(II) from aqueous solution by chitosan-lead ion-imprinted polymer network, Chemosphere, 240 (2020) 124772, doi: 10.1016/j.chemosphere.2019.124772.

[6] R. Reshmy, E. Philip, A. Madhavan, A. Pugazhendhi, R. Sindhu, R. Sirohi, M.K. Awasthi, A. Pandey, P. Binod, Nanocellulose as green material for remediation of hazardous heavy metal contaminants, J. Hazard. Mater., 424 (2022) 127516, doi: 10.1016/j.jhazmat.2021.127516.

[7] P.S. Bakshi, D. Selvakumar, K. Kadirvelu, N.S. Kumar, Chitosan as an environment friendly biomaterial – a review on recent modifications and applications, Int. J. Biol. Macromol., 150 (2020) 1072–1083.

[8] N. Nematidil, M. Sadeghi, S. Nezami, H. Sadeghi, Synthesis and characterization of Schiff-base based chitosan-g-glutaraldehyde/NaMMTNPs-APTES for removal Pb^{2+} and Hg^{2+} ions, Carbohydr. Polym., 222 (2019) 114971, doi: 10.1016/j.carbpol.2019.114971.

[9] S. Shahraki, H.S. Delarami, F. Khosravi, R. Nejat, Improving the adsorption potential of chitosan for heavy metal ions using aromatic ring-rich derivatives, J. Colloid Interface Sci., 576 (2020) 79–89.

[10] R. Huang, N. Shao, L. Hou, X. Zhu, Fabrication of an efficient surface ion-imprinted polymer based on sandwich-like graphene oxide composite materials for fast and selective removal of lead ions, Colloids Surf., A, 566 (2019) 218–228.

[11] D.G. Trikkaliotis, A.K. Christoforidis, A.C. Mitropoulos, G.Z. Kyzas, Adsorption of copper ions onto chitosan/poly(vinyl alcohol) beads functionalized with poly(ethylene glycol), Carbohydr. Polym., 234 (2020) 115890, doi: 10.1016/j.carbpol.2020.115890.

[12] W.S. Wan Ngah, L.C. Teong, R.H. Toh, M.A.K.M. Hanafiah, Comparative study on adsorption and desorption of Cu(II) ions by three types of chitosan–zeolite composites, Chem. Eng. J., 223 (2013) 231–238.

[13] S. Brundavanam, G.E.J. Poinern, D. Fawcett, Kinetic and adsorption behaviour of aqueous Fe^{2+}, Cu^{2+} and Zn^{2+} using a 30 nm hydroxyapatite based powder synthesized via a combined ultrasound and microwave based technique, Am. J. Mater. Sci., 5 (2015) 31–40.

[14] Y.M. Issa, H.B. Hassib, H.E. Abdelaal, ^{1}H NMR, ^{13}C NMR and mass spectral studies of some Schiff bases derived from 3-amino-1,2,4-triazole, Spectrochim. Acta, Part A, 74 (2009) 902–910.

[15] H.L. Vasconcelos, E. Guibal, R. Laus, L. Vitali, V.T. Fávere, Competitive adsorption of Cu(II) and Cd(II) ions on spray-dried chitosan loaded with Reactive Orange 16, Mater. Sci. Eng., C, 29 (2009) 613–618.

[16] R. Hassan, H. Arida, M. Montasser, N. Abdel Latif, Synthesis of new Schiff base from natural products for remediation of water pollution with heavy metals in industrial areas, J. Chem., 2013 (2013) 240568, doi: 10.1155/2013/240568.

[17] V. Pakade, E. Cukrowska, J. Darkwa, N. Torto, L. Chimuka, Selective removal of chromium(VI) from sulphates and other metal anions using an ion-imprinted polymer, Water SA, 37 (2011) 529–538.

[18] H. Liu, D. Kong, W. Sun, Q. Li, Z. Zhou, Z. Ren, Effect of anions on the polymerization and adsorption processes of Cu(II) ion-imprinted polymers, Chem. Eng. J., 303 (2016) 348–358.

[19] S. Gokila, T. Gomathi, P.N. Sudha, S. Anil, Removal of the heavy metal ion chromium(VI) using chitosan and alginate nanocomposites, Int. J. Biol. Macromol., 104 (2017) 1459–1468.

[20] L.D. Mafu, B.B. Mamba, T.A.M. Msagati, Synthesis and characterization of ion-imprinted polymeric adsorbents for the selective recognition and removal of arsenic and selenium in wastewater samples, J. Saudi Chem. Soc., 20 (2016) 594–605.

[21] M. Abd El-Latif, A.M. Ibrahim, M. El-Kady, Adsorption equilibrium, kinetics and thermodynamics of methylene blue from aqueous solutions using biopolymer oak sawdust composite, J. Am. Sci., 6 (2010) 267–283.

[22] J.C. Igwe, A. Abia, Studies on the effects of temperature and particle size on bioremediation of As(III) from aqueous solution using modified and unmodified coconut fiber, Global J. Environ. Res., 1 (2007) 22–26.

[23] H.-T. Fan, X.-T. Sun, Z.-G. Zhang, W.-X. Li, Selective removal of lead(II) from aqueous solution by an ion-imprinted silica sorbent functionalized with chelating N-donor atoms, J. Chem. Eng. Data, 59 (2014) 2106–2114.

[24] V.T. Le, M.U. Dao, H.S. Le, D.L. Tran, V.D. Doan, H.T. Nguyen, Adsorption of Ni(II) ions by magnetic activated carbon/chitosan beads prepared from spent coffee grounds, shrimp shells and green tea extract, Environ. Technol., 41 (2020) 2817–2832.

[25] Y. He, P. Wu, W. Xiao, G. Li, J. Yi, Y. He, C. Chen, P. Ding, Y. Duan, Efficient removal of Pb(II) from aqueous solution by a novel ion imprinted magnetic biosorbent: adsorption kinetics and mechanisms, PLoS One, 14 (2019) e0213377, doi: 10.1371/journal.pone.0213377.

[26] Z. Zhou, D. Kong, H. Zhu, N. Wang, Z. Wang, Q. Wang, W. Liu, Q. Li, W. Zhang, Z. Ren, Preparation and adsorption characteristics of an ion-imprinted polymer for fast removal of Ni(II) ions from aqueous solution, J. Hazard. Mater., 341 (2018) 355–364.

[27] Z. Li, W. Kou, S. Wu, L. Wu, Solid-phase extraction of chromium(III) with an ion-imprinted functionalized attapulgite sorbent prepared by a surface imprinting technique, Anal. Methods, 9 (2017) 3221–3229.

[28] X. Xu, M. Wang, Q. Wu, Z. Xu, X. Tian, Synthesis and application of novel magnetic ion-imprinted polymers for selective solid phase extraction of cadmium(II), Polymers, 9 (2017) 360, doi: 10.3390/polym9080360.

[29] M.J. Kuras, E. Więckowska, Synthesis and characterization of a new copper(II) ion-imprinted polymer, Polym. Bull., 72 (2015) 3227–3240.

[30] Y. Jiang, D. Kim, Effect of solvent/monomer feed ratio on the structure and adsorption properties of Cu^{2+}-imprinted microporous polymer particles, Chem. Eng. J., 166 (2011) 435–444.

[31] A. Chaipuang, C. Phungpanya, C. Thongpoon, K. Watla-iad, P. Inkaew, T. Machan, O. Suwantong, Synthesis of copper(II) ion-imprinted polymers via suspension polymerization, Polym. Adv. Technol., 29 (2018) 3134–3141.

[32] J. Fu, X. Wang, J. Li, Y. Ding, L. Chen, Synthesis of multi-ion-imprinted polymers based on dithizone chelation for simultaneous removal of Hg^{2+}, Cd^{2+}, Ni^{2+} and Cu^{2+} from aqueous solutions, RSC Adv., 6 (2016) 44087–44095.

[33] A. Masykur, A.H. Wibowo, Salsabilah, Preparation of Cu(II) ion-imprinted based on carboxymethyl chitosan and application as

adsorbent of Cu(II) ion, IOP Conf. Ser.: Mater. Sci. Eng., 13th Joint Conference on Chemistry (13th JCC) 7–8 September 2018, Semarang, Indonesia, 509 (2019) 012001.

[34] C.-W. Oo, H. Osman, S. Fatinathan, M.A.M. Zin, The uptake of copper(II) ions by chelating Schiff base derived from 4-aminoantipyrine and 2-methoxybenzaldehyde, Int. J. Nonferrous Metall., 2 (2013), doi: 10.4236/ijnm.2013.21001.

[35] K. Tekin, L. Uzun, Ç.A. Şahin, S. Bektaş, A. Denizli, Preparation and characterization of composite cryogels containing imidazole group and use in heavy metal removal, React. Funct. Polym., 71 (2011) 985–993.